Coupled Simulation of the Flue Gas and Process Gas Side of a Steam Cracker Convection Section

Sandra C.K. De Schepper, Geraldine J. Heynderickx, and Guy B. Marin
Laboratory for Chemical Technology, Ghent University, Krijgslaan 281 (S5), B-9000 Ghent, Belgium

DOI 10.1002/aic.11927
Published online September 14, 2009 in Wiley InterScience (www.interscience.wiley.com).

A coupled simulation of the flue gas and process gas side of the convection section of a steam cracker is performed, making use of the CFD software package Fluent. A detailed overview of the operating mode of the different heat exchangers suspended in the convection section is obtained. The asymmetric inlet flow field of the flue gas in the convection section, and the radiation from the convection section walls leads to large differences in outlet temperatures of the tubes located in the same row. The flow fields and temperature fields in the tubes of a single heat exchanger differ significantly with e.g., outlet temperatures of the hydrocarbon-steam mixture ranging from 820 K to 852 K. Moreover, the simulations reveal the presence of hot spots on the lowest tube row, possibly causing fouling. © 2009 American Institute of Chemical Engineers *AIChE J,* 55: 2773–2787, 2009

Keywords: steam cracking, computational fluid dynamics (CFD), heat transfer

Introduction

Steam cracking, one of the most important processes in petrochemical industry, converts a hydrocarbon feedstock into more valuable products such as ethylene and propylene. There is an increasing demand for ethylene, propylene and their derivatives, mainly because of the high number of applications of these products in the polymer industry.[1]

A steam cracker is composed of two sections: a radiation section and a convection section. The radiation section is a furnace heated with side-wall radiation burners and/or long flame burners in the floor, supplying the necessary heat for the endothermal cracking process. In this section, over 90% of the heat transfer from the flue gas and the furnace walls to the reactor coils is radiative. Hence, the radiation section is an empty volume with a number of vertically suspended tubular reactor coils in the middle of this section. The hydrocarbon-steam mixture is cracked in the coils, with a residence time of typically 0.1–0.5 s, and temperatures from ranging from 900 to 1200 K. The flue gas flows along these coils. A complete and detailed simulation of the radiation section requires a coupled simulation of both the furnace and the reactor coils, as the conditions in both reactor coils and furnace influence one another.[2,3,4,5,6] In the past, the cracking reactions in the coils, and the radiation in the furnace have received extended research attention.[7,8,9] Typical furnace dimensions, operating conditions and simulation results for the radiation section are presented by Heynderickx et al.[3] In the convection section, the energy remaining in the flue gas leaving the radiation section is used to preheat and vaporize the hydrocarbon feedstock, to overheat the steam that is mixed with the hydrocarbons and to overheat the hydrocarbon-steam mixture before entering the cracking coils in the radiation section. The major part of the heat transfer is due to convection, as the flue gas temperature is considerably lower than in the radiation section: 1400 K vs. 2000 K. As a result, the convection section is filled with a large number of horizontally suspended heat exchanger tubes resulting in a cross flow configuration of flue gas and process gas.

As for the radiation section, a complete and detailed simulation of the convection section will require a coupled simulation of the flue gas side and the internals of the heat

Additional Supporting Information may be found in the online version of this article.

Correspondence concerning this article should be addressed to G. J. Heynderickx at Geraldine.heynderickx@ugent.be.

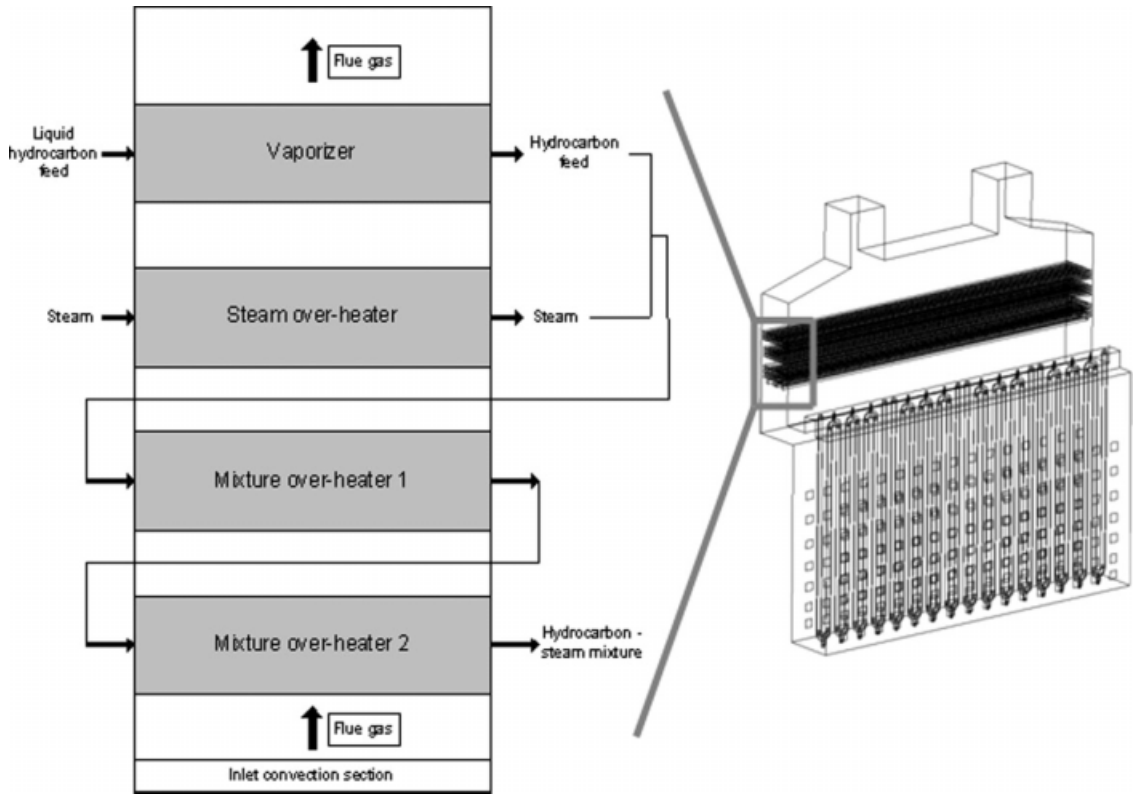

Figure 1. Configuration of the convection section of a steam cracker.

exchanger tubes. Unlike the radiation section, the simulation of the convection section of a steam cracker has not received any research attention yet.

Comparable to the coking in the tubes of the radiation section,[2,10,11] fouling can occur in the tubes of the convection section. A coupled simulation of the flue gas side and the process gas side of the convection section is required to analyze and solve the resulting problems. Such a simulation can reveal e.g., the presence of hot spots on the convection section tube skins, possibly causing fouling. In this work, such a coupled simulation is performed in view of a later fouling study in the convection section tubes. The approach of a coupled simulation was proven to be a useful tool to determine the fouling and, subsequently, the run length of an ethane cracker by Heynderickx and Froment.[13] Accounting for the fouling in the reactor coils, a time-dependent coupled simulation of the radiation section of an ethane cracker was performed. The industrial and calculated run-length agreed within one day.[13]

At first, a complete simulation of the convection section, making use of the process simulator Aspen[14] is performed. However, the use of this simulator is not satisfactory for a detailed study of the phenomena occurring in the convection section due to e.g., evaporation, hot spots or fouling. Hence, different software has to be used to study local phenomena in specific zones of the convection section. The commercial CFD software Fluent[15] has the capabilities to perform a detailed study of the operation of the convection section. A coupled simulation of the convection section, i.e., flue-gas side and process gas side, will be performed making use of Fluent.[15] First, a presentation of the convection section geometry and the applied methodology is given. Next, the models required to perform such a coupled simulation of the convection section are presented. It is explained why given models are selected to perform specific parts of the simulation work. Finally, the simulation results for the flue gas side and each of the heat exchangers are described.

Geometry of the convection section of a steam cracker

The convection section of a steam cracker is positioned above the radiation section, as can be seen on Figure 1. The convection section is filled with a large number, 112 in this work, of horizontally suspended heat exchanger tubes over which the flue gas flows. An overview of the position of the different heat exchangers in the convection section is also found in Figure 1. In this work, a convection section with four heat exchangers is calculated. In the top of the convection section, where the flue gas temperature has dropped to its lowest value of about 950 K, a heat exchanger is suspended in which the liquid hydrocarbon feed is partially vaporized. In the heat exchanger suspended below the vaporizer, steam is overheated. After mixing the outlet streams of both these heat exchangers, the hydrocarbon-steam mixture flows through a third heat exchanger. In this heat exchanger, the hydrocarbons that have not yet been vaporized after the mixing with the overheated steam are vaporized. Finally, in the last heat exchanger, the completely gaseous hydrocarbon-steam mixture is further overheated. As the latter process requires the highest flue gas temperatures, this heat exchanger is suspended near the flue gas inlet of the

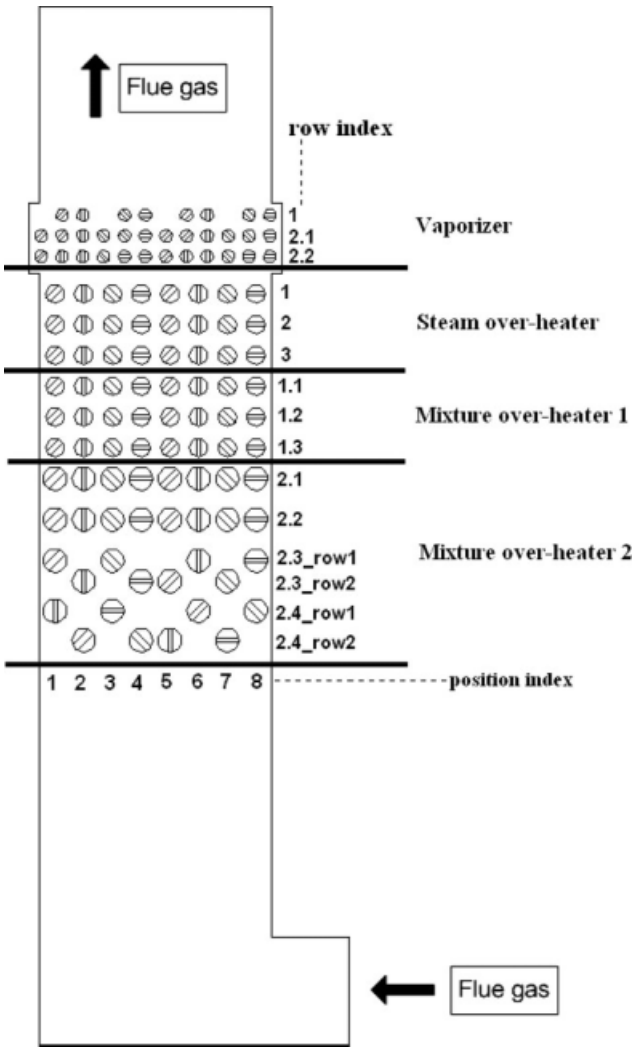

Figure 2. Cross-section of the convection section with indication of the heat exchangers and the tube position.

convection section where flue gas coming from the radiation section has its highest-temperature value, typically 1450 K.

Figure 2 shows a cross-section of the convection section with indication of the different heat exchangers and the position of the tubes in the convection section box. The liquid hydrocarbon feed is distributed over eight parallel tubes making a number of horizontal passes, typically 11, through the convection section (follow the symbols in Figure 2 to follow the flow from tube to tube). Since the total flow of the steam and hydrocarbon-steam mixture is divided over eight different tubes, located on a different position in the convection section, see Figure 2, the complete simulation all these heat exchangers requires the calculation of all eight positions.

The horizontal passes are connected by horizontal, vertical or oblique U-tube bends. These bends are located outside the convection section. The tube geometry for the different heat exchangers varies in terms of number of horizontal passes through the convection section, a vertical, horizontal or oblique U-bend between those passes and varying tube diameters. The construction of the central heat exchangers, i.e., the steam over-heater and mixture over-heater 1, is simple. Each of the eight heat exchanger tubes makes three horizontal passes connected by vertical U-tube bends. The heat exchanger with the most complicated geometry is the lower one, i.e., the mixture over-heater 2. The two last passes of the heat exchanger tubes are geometrically noncorresponding (see Figure 2).

The heat flux profile along each tube pass differs depending on the position of the tube in the tube bundle and the position of the tube bundle in the convection section. Thus, a coupled simulation of the convection section requires that every tube pass of each heat exchanger is simulated separately. The simulation results will clearly show the need for such a complete simulation, as the obtained fields are extremely asymmetric and nonuniform.

The simulation of all heat exchanger tubes separately requires a detailed working scheme and is extremely time-consuming. In each simulation, the specific boundary conditions for the tube under consideration are to be imposed. This implies that for the calculation of the flow and temperature field in one heat exchanger tube, the correct inlet conditions and heat flux profile should be applied. Moreover, in the simulation of the flue gas side, the inner tube wall temperatures for each of the tubes should be defined as thermal boundary condition. The latter implies that, in total, 112 temperature profiles should be taken into account. A graphical representation of the applied numbering scheme can be found in Figure 2. In this scheme, each tube has a unique code, based on the name of the heat exchanger and the position of the tube in the convection section. For example, the tube with code steam over-heater_row1_position1 corresponds with the first horizontal tube pass of the steam over-heater tube located at position 1, as can be seen on Figure 2. The codes of these tubes are used in the simulation of the flue gas side as well as the process gas side.

Calculation of the Convection Section by Means of Fluent

Methodology

The different steps in a coupled simulation of the flue gas side and the process gas side of the convection section are presented in Figure 3. From the simulation of the flue gas side, the heat-flux profiles to the different tubes of the four heat exchangers are calculated. Based on these profiles, the phenomena in the tubes of the heat exchangers, i.e., vaporization, steam overheating and heating of the hydrocarbon-steam mixture are calculated. These simulations provide the temperatures of the internal tube skin of the different tubes. Based on these temperature profiles, a new flue gas simulation is performed. The former steps are repeated until convergence is reached. Using this approach, a complete coupling of both sides of the convection section is obtained.

A correct calculation of the heating and vaporization of the hydrocarbons in the vaporizer involves the simulation of a flow boiling process. The latter is still a major challenge in computational fluid dynamics. During the evaporation, the liquid to vapor fraction changes continuously, resulting in different two-phase flow regimes.[16] Although commercial

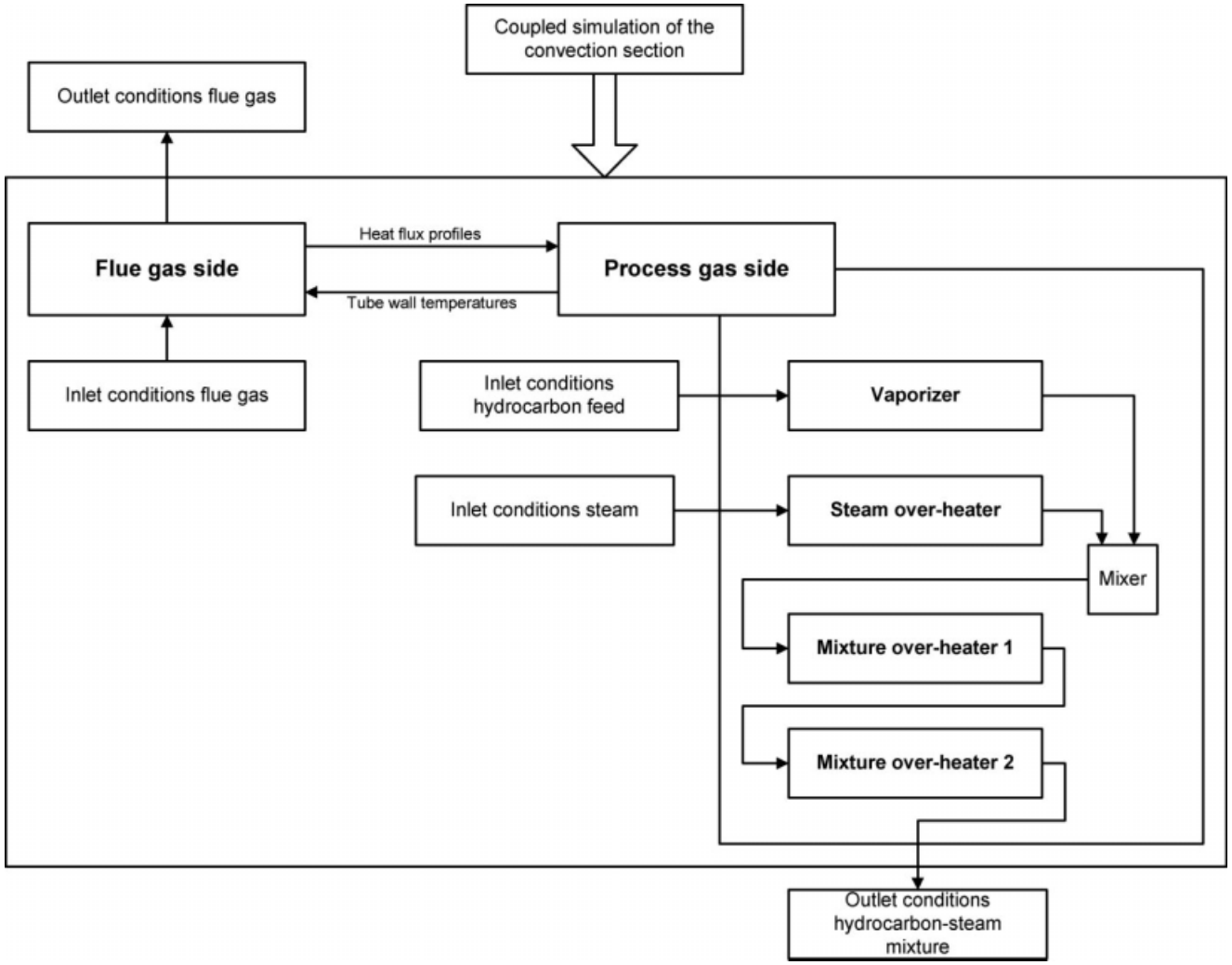

Figure 3. General scheme indicating the methodology to perform a coupled simulation of the convection section.

CFD software packages dispose over several models to simulate the two-phase vapor–liquid flow,[17] it needs to be confirmed whether the predicted two-phase-flow regime corresponds with the actual flow regime for a given liquid-to-vapor ratio. The commercial software package Fluent[15] used in this work, was found to give meaningful results.[18] On the other hand, Fluent[15] does not allow simulating the evaporation process itself. As such, the state-of-the-art led to the use of the Aspen calculation results for the simulation of the vaporizer process gas. Also, as fouling problems are not to be expected in the low-temperature tubes of the vaporizer, the use of the Aspen calculation results for the vaporizer in the Fluent simulations is justified. Even with this simplified simulation of the vaporizer, a coupled simulation of the convection section of a steam cracker remains extremely time-consuming. The calculations are performed on a personal computer with dual 3.0 GHz processor and 4 GB RAM, using 4 months of calculation time. Convergence over the complete convection section is reached after four consecutive simulations of the flue gas side and the process gas side. The results are presented in the section Simulation Results.

Models

Reynolds averaged Navier-Stokes equations

To obtain the mass, velocity and temperature field of a fluid flowing in the computational domain under consideration, a set of conservation equations, the well known Navier-Stokes equations, must be solved.

Both the flue gas coming from the radiation section as the hydrocarbon feed and steam are introduced at a high velocity, causing a highly turbulent flow regime. A correct simulation of these turbulence effects is needed. Turbulent flows are characterized by fluctuating velocity fields. The velocity fluctuations do not only mix the transported quantities such as momentum, energy and species concentrations, but cause fluctuations of the latter quantities as well. Since these fluctuations can be of small scale and high frequency, it is computationally too expensive to simulate them directly. To remove these small-scale fluctuations from the set of conservation equations, the instantaneous conservation equations are averaged. This results in a modified set of equations, computationally less expensive to solve. Transformation of

Table 1. Reynolds Averaged Navier-Stokes Equations

Reynolds Averaged Navier-Stokes equations
$$\frac{\partial}{\partial t}(\rho) + \sum_{i=1}^{3} \frac{\partial}{\partial x_i} \cdot (\rho \bar{u}_i) = S_M \quad (1)$$
$$\frac{\partial}{\partial t}(\rho \bar{u}_i) + \sum_{j=1}^{3} \frac{\partial}{\partial x_j} \cdot \left(\rho \bar{u}_i \bar{u}_j\right) = -\frac{\partial p}{\partial x_i} + \sum_{j=1}^{3} \frac{\partial}{\partial x_j}\left[\mu\left(\frac{\partial \bar{u}_i}{\partial x_j} + \frac{\partial \bar{u}_j}{\partial x_i} - \frac{2}{3}\delta_{ij}\sum_{l=1}^{3}\frac{\partial \bar{u}_l}{\partial x_l}\right)\right] + \sum_{j=1}^{3}\frac{\partial}{\partial x_j}\left(-\rho\overline{u_i' u_j'}\right) + S_{F,i} \quad (2)$$
$$\frac{\partial}{\partial t}(\rho E) + \sum_{j=1}^{3}\frac{\partial}{\partial x_j}\left(\rho E \bar{u}_j\right) = \sum_{i=1}^{3}\sum_{j=1}^{3}\left(\frac{\partial}{\partial x_j}\left(\tau_{ij} - \rho\overline{u_i' u_j'}\right)\bar{u}_i\right) - \sum_{j=1}^{3}\frac{\partial}{\partial x_j} q_j + S_E \quad (3)$$
Reynolds stresses
$$-\rho\overline{u_i' u_j'} = \mu_{\text{turb}}\left(\frac{\partial \bar{u}_i}{\partial x_j} + \frac{\partial \bar{u}_j}{\partial x_i}\right) - \frac{2}{3}\left(\rho k + \mu_{\text{turb}}\sum_{l=1}^{3}\frac{\partial \bar{u}_l}{\partial x_l}\right)\delta_{ij} \quad (4)$$

the instantaneous flow equations to conservation equations in the averaged variables, results in the well-known Reynolds-Averaged Navier-Stokes equations (the so-called RANS equations), which may be found in Table 1 (Eqs.1 to 3). More detailed information concerning these equations and an analysis of the different contributions may be found in Anderson[19] and Versteeg and Malalasekera.[20]

The Reynolds-averaged Navier-Stokes equations describe the transport of the averaged flow quantities, with the whole range of the turbulence scales being modeled. However, due to the averaging, a number of additional unknown variables are introduced in the equations. These unknown variables, called Reynolds stresses (see Eq. 4 in Table 1), must be modeled in terms of known quantities, making use of so-called "closure models", known as turbulence models.[20] For the simulation of the convection section, that is the flue gas side on the one hand, and the different heat exchangers on the other hand, different turbulence models have been applied, as described and justified in the next section.

Turbulence modeling

The selection of the appropriate turbulence model from the available turbulence models for the application at hand is important for the simulations to be performed. The implications of the selection of a given model must be adequately understood. It should be kept in mind that a more complex model does not necessarily imply that more correct results are obtained. Therefore, for the turbulence modeling at the flue gas side and in the different heat exchangers located in the convection section, different models have been applied. More specifically, the phenomena taking place in the location under consideration determines the selection of the most appropriate turbulence model. In what follows, the turbulence models will be explained and the choice will be justified.

Turbulence Model for the Simulation of the Flue-Gas Side: Standard k-ε *model.* Generally, the two-equation standard k-ε model is recommended as a baseline model. For the simulation of the flue gas side of the convection section, this turbulence model has been used. The simplest complete turbulence model is a two-equation model in which the solution of two conservation equations with corresponding constitutive equations, see Tables 1 and 2, suffices to independently determine the turbulent velocity and length scales. The standard k-ε model falls within this class of turbulence models and has become the workhorse of practical engineering flow calculations since it was proposed by Launder and Spalding.[21] *Robustness, economy, and reasonable accuracy for a wide range of turbulent flows explain its popularity in industrial flow and heat-transfer simulations.*

By application of the Boussinesq hypothesis,[20] the Reynolds stresses, see Eq. 4 in Table 1, are related to the mean velocity gradients. A value for the turbulent viscosity μ_{turb} is needed to determine the Reynolds stresses. Using the standard k-ε model, the calculation of the turbulent viscosity is computationally nonexpensive. The transport equations for the turbulent kinetic energy k, and the viscous dissipation of the turbulent kinetic energy ε are solved, see Eqs. 5 and 6 in Table 2. The turbulent viscosity is then calculated as a function of k and ε, see Eq. 8 in Table 2. It should be remarked that, in the derivation of the k-ε model, it is assumed that the flow is fully turbulent, and the effects of molecular viscosity are negligible. The standard k-ε model, is, therefore, only valid for fully turbulent flows. Since the flow of the flue gas in the convection section is fully developed and

Table 2. Governing Equations of the Standard *k*-ε Model

Standard k- ε model

$$\frac{\partial}{\partial t}(\rho k)+\sum_{j=1}^{3}\frac{\partial}{\partial x_j}\left(\rho k\bar{u}_j\right)=\sum_{j=1}^{3}\frac{\partial}{\partial x_j}\left[\left(\mu+\frac{\mu_{\text{turb}}}{\sigma_k}\right)\frac{\partial k}{\partial x_j}\right]+\bar{P}_k-\rho\varepsilon \tag{5}$$

$$\frac{\partial}{\partial t}(\rho\varepsilon)+\sum_{j=1}^{3}\frac{\partial}{\partial x_j}\left(\rho\varepsilon\bar{u}_j\right)=\sum_{j=1}^{3}\frac{\partial}{\partial x_j}\left[\left(\mu+\frac{\mu_{\text{turb}}}{\sigma_\varepsilon}\right)\frac{\partial\varepsilon}{\partial x_j}\right]+C_{1\varepsilon}\frac{\varepsilon}{k}\bar{P}_k-C_{2\varepsilon}\rho\frac{\varepsilon^2}{k} \tag{6}$$

$$\bar{P}_k=\sum_{i=1}^{3}\sum_{j=1}^{3}\left[\left(\mu_{\text{turb}}\left(\frac{\partial\bar{u}_i}{\partial x_j}+\frac{\partial\bar{u}_j}{\partial x_i}-\delta_{ij}\sum_{l=1}^{3}\frac{2}{3}\frac{\partial\bar{u}_l}{\partial x_l}\right)-\frac{2}{3}\rho k\delta_{ij}\right)\frac{\partial\bar{u}_j}{\partial x_i}\right] \tag{7}$$

$$\mu_{\text{turb}}=\rho C_\mu\frac{k^2}{\varepsilon} \tag{8}$$

highly turbulent, the standard *k*-ε model suffices for the simulation of the flue gas side.

Turbulence Model for the Simulation of the Steam-Overheater and Mixture Over-Heater 2: ReNormalization Group (RNG) k-ε Model. For the calculation of the flow field inside the tubes of the steam over-heater and mixture over-heater 2, see Figure 1, another turbulence model has been applied. First, the tubes of these heat exchangers are filled with a one-phase vapor flow. Second, the horizontal heat exchanger tubes in the convection section are connected by U-bends. As a result, swirling flow is observed in these bends. The RNG *k*-ε model[22] provides a swirl modification option to the standard *k*-ε model, which accounts for the effects of swirl or rotation in turbulent flow. Therefore, the RNG *k*-ε model has been chosen as turbulence model for the simulation of both these heat exchangers. Knowing the strengths and weaknesses of the standard *k*-ε model, different adjusted models to improve its performance have been introduced in literature.[23,24] The RNG *k*-ε model is such a variant of the standard *k*-ε model. The RNG *k*-ε model was derived using a rigorous statistical technique called the renormalization group theory.[25] Its concept is similar to the standard *k*-ε model, but includes some refinements.

Again, by application of the Boussinesq hypothesis,[20] the Reynolds stresses (see Eq. 4 in Table 1) are related to the mean velocity gradients. As mentioned before, the turbulent viscosity needs to be determined. In the RNG version of the *k*-ε model of turbulence, the turbulent viscosity is related to turbulent kinetic energy k, and the viscous dissipation of turbulent kinetic energy ε by the following differential equation[22]

$$\mathrm{d}\left(\frac{\rho^2 k}{\sqrt{\varepsilon\mu}}\right)=1.72\frac{\upsilon}{\sqrt{\upsilon^3-1+C_\upsilon}}\mathrm{d}\upsilon \tag{9}$$

where $\upsilon=\mu+\mu_{\text{turb}}/\mu$.

Equation 9 in the RNG *k*-ε model replaces Eq. 8 in Table 2 for the standard *k*-ε model. The aforementioned equation must be integrated to obtain an accurate description of the dependence of the effective turbulent transport on the effective Reynolds number. This allows the RNG *k*-ε turbulence model to better handle low-Reynolds-number and near-wall flows. In the high-Reynolds-number limit, i.e., for fully developed turbulent flow, Eq. 9 becomes

$$\mu_{\text{turb}}=\rho C_\mu\frac{k^2}{\varepsilon} \tag{10}$$

or the well-known Eq. 8 in Table 2 for the standard *k*-ε model.

Solving Eq. 9 requires values for k and ε. Local values of k and ε can be obtained by solving the transport equations for these variables, that is the equations of the standard *k*-ε model, see Eqs. 5 and 6 in Table 2. However, the values of the model parameters differ, as found in Table 3. It can be seen that σ_k and σ_ε, the effective Prandtl numbers for k and ε, are computed from a constitutive equation that was analytically derived using the RNG theory, contrary to the standard *k*-ε model where they have a constant value.

Turbulence, in general, is affected by rotation or swirl in the mean flow. The RNG *k*-ε model provides an option to account for the effects of swirl or rotation by modifying the turbulent viscosity as compared to the standard *k*-ε model. The RNG *k*-ε model is more appropriate to model the effects of rapid strain and streamline curvature than the standard *k*-ε model, which explains the superior performance of the RNG *k*-ε model for given flow conditions.[26,27] The main difference between the standard and RNG version of the *k*-ε model is found in the values for the parameters used in the transport equation for the turbulent energy dissipation rate ε, see Eq. 6 in Table 2. In large strain rate flows, the RNG *k*-ε model predicts a lower turbulent viscosity, i.e., a larger ε and smaller k, than the standard *k*-ε model. Although the RNG *k*-ε model has been found to perform better than the standard model for flows with high streamline curvature and vortex shedding, the RNG *k*-ε

Table 3. Model Constants for the Standard and RNG k-ε Turbulence Model

Model constant	Standard k-ε model	RNG k-ε model
C_μ	0.09	0.0845
$C_{1\varepsilon}$	1.44	1.42
$C_{2\varepsilon}$	1.92	$1.68+\frac{C_\mu\rho\eta^3(1-\eta/4.38)}{1+0.012\eta^3}\cdot\cdot\eta=\frac{k\sqrt{P_k/\mu_{turb}}}{\varepsilon}$
σ_k	1.00	$\left\|\frac{1/\sigma-1.3929}{0.3929}\right\|^{0.6321}\left\|\frac{1/\sigma+2.3929}{3.3929}\right\|^{0.3679}=\frac{\mu}{\mu_{turb}}$
σ_ε	1.30	$\left\|\frac{1/\sigma-1.3929}{0.3929}\right\|^{0.6321}\left\|\frac{1/\sigma+2.3929}{3.3929}\right\|^{0.3679}=\frac{\mu}{\mu_{turb}}$

model has not yet been validated as extensively as the standard k-ε model.[24]

Turbulence Model for the Simulation of the Mixture Over-Heater 1: Reynolds Stress Model. In the mixture over-heater 1, the hydrocarbons remaining in the liquid phase are first vaporized, and next the hydrocarbon-steam mixture is further overheated. Due to the presence of the small liquid hydrocarbon droplets at the entrance of this heat exchanger, spray flow is observed in the tubes of this heat exchanger. The simulation of the droplet trajectories through the tubes requires a different modeling approach, and, thus, a specialized turbulence model. For the hydrocarbon-steam mixture in mixture over-heater 1 where hydrocarbon liquid is still present, the more elaborate Reynolds stress model (RSM)[28] is selected to describe the effects of turbulence. Since the RSM turbulence model accounts for the effects of streamline curvature, swirl, rotation and rapid changes in strain rate in a more rigorous manner than the one-equation and two-equation turbulence models, it has greater potential to give an accurate prediction for complex flows.[29] It was found in literature that the RSM turbulence model is the most appropriate model for the simulation of cyclone flows and highly swirling flows.[30,31] Moreover, this turbulence model is extensively used when intending to simulate particle trajectories. Consequently, the RSM turbulence model will be used for the simulation of the mixture over-heater 1 where part of the hydrocarbon feed is still in the liquid phase as small droplets.

The Reynolds stress model (RSM) is the most elaborate turbulence model that the commercial CFD software package Fluent[15] provides. Abandoning the isotropic eddy-viscosity hypothesis, the RSM turbulence model closes the Reynolds-averaged Navier-Stokes equations by solving transport equations for the Reynolds stresses, together with a transport equation for the turbulent kinetic energy dissipation rate. Thus, seven additional transport equations must be solved when calculating the three-dimensional (3-D) flow field.

The exact form of the Reynolds stress transport equations to be solved is derived by taking the moments of the exact momentum equation. Unfortunately, several of the terms in the exact equations are unknown and modeling assumptions are required in order to close the Reynolds stress transport equations. The exact transport equation for the Reynolds stresses $\rho\overline{u_i'u_j'}$ may be written as follows

$$\underbrace{\frac{\partial}{\partial t}\left(\rho\overline{u_i'u_j'}\right)}_{\text{Local time derivative}}+\underbrace{\frac{\partial}{\partial x_k}\left(\rho u_k\overline{u_i'u_j'}\right)}_{C_{ij}\equiv\text{Convection}}$$
$$=\underbrace{-\frac{\partial}{\partial x_k}\left[\rho\overline{u_i'u_j'u_k'}+\overline{p\left(\delta_{kj}u_i'+\delta_{ik}u_j'\right)}\right]}_{D_{T,ij}\equiv\text{Turbulent diffusion}}+\underbrace{\frac{\partial}{\partial x_k}\left[\mu\frac{\partial}{\partial x_k}\left(\overline{u_i'u_j'}\right)\right]}_{D_{L,ij}\equiv\text{Molecular diffusion}}$$
$$\underbrace{-\rho\left(\overline{u_i'u_k'}\frac{\partial u_j'}{\partial x_k}+\overline{u_j'u_k'}\frac{\partial u_i'}{\partial x_k}\right)}_{P_{ij}\equiv\text{Stress production}}\underbrace{-\rho\beta\left(g_i\overline{u_j'\theta}+g_j\overline{u_i'\theta}\right)}_{G_{ij}\equiv\text{Buoyancy production}}$$
$$+\underbrace{\overline{p\left(\frac{\partial u_i'}{\partial x_k}+\frac{\partial u_j'}{\partial x_i}\right)}}_{\varphi_{ij}\equiv\text{Pressure strain}}\underbrace{-2\mu\overline{\frac{\partial u_i'}{\partial x_k}\frac{\partial u_j'}{\partial x_k}}}_{\varepsilon_{ij}\equiv\text{Dissipation}}\quad(12)$$

For a detailed description of the different contributions in the Eq.12 and their modeling, reference is made to Ranade[24] and the User's Guide of Fluent.[15] The terms describing turbulent diffusion, buoyancy production, pressure strain and dissipation are unknown, and, thus, need modeling to close the Reynolds stress transport equations. The dissipation rate ε is computed with a model transport equation similar to that used in the standard k-ε model (see Eq. 6 in Table 2).

As already remarked, the RSM turbulence model accounts for the effects of streamline curvature, swirl, rotation and rapid changes in strain rate in a rigorous manner. As such, it has more potential to give accurate predictions for complex flows.[29] However, the reliability of RSM predictions is still limited, due to the closure assumptions used for the various contributions in the exact transport equations for the Reynolds stresses. The RSM turbulence model does not always guarantee that simulation results are superior to those obtained with a simpler model, especially when accounting for the additional computational expense.[24] However, use of the Reynolds stress model is required when the flow features of interest are the result of anisotropy in the Reynolds stresses.

It can be concluded that the RSM turbulence model is the most general model of all classical turbulence models. It performs well for many complex flows including curved flows. However, due to the necessity to solve seven additional transport equations next to the RANS equations, this model is computationally very expensive. Moreover, this model has not yet been widely validated.[24]

Radiation modeling

The simulation of the radiative heat transfer in the convection section is done making use of the discrete ordinate model (DOM).[15] By applying this model, the radiation of hot-flue gases is taken into account. The DOM transforms the radiative transfer equation into a transport equation for radiation intensity.[32,33] The equation is then solved using the same technique as applied for the other transport equations. The absorption coefficient of the flue gas is calculated using the Hottel/Leckner model for H_2O and CO_2 radiation,[34,35] based on the known partial pressure of the flue gas components, temperature, and the approximate path length of beams. The DOM focuses on the path length of the beams, because the absorption coefficient strongly depends on the

"volume" of the radiative gas. Starting from several possibilities, considering the path lengths between the convection section walls, between the tubes and between the convection section walls and the tubes, the longest path length is used, giving reasonable results in the open volume below the tube banks, and resulting in low radiation in the tube bank region. This is in good agreement with industrial information, stating that the radiation is intensive only for the lower tubes in the convection section. The absorption coefficient of the flue gas is implemented into the DOM as a polynomial function of temperature. Remark that radiation is strongly temperature-dependent. In the bottom of the convection section, flue gas temperatures are still high, and the contribution of radiation to the total heat transfer is still considerable. However, as the flue gas temperature drops, the radiative contribution drops rapidly.

Physical properties

The number of chemical components that can be selected in Fluent[15] is limited and the temperature dependence of the physical properties of these components making up the flue gas, the hydrocarbon feed and the hydrocarbon-steam mixture can not be accounted for. To solve this shortcoming a simplified simulation of the convection section is performed using the commercial code Aspen.[14] The results of the latter simulation are used to construct polynomial functions expressing the variation of physical properties with temperature. The latter will be used in the Fluent[15] simulation of the convection section. An overview of the polynomial functions is found in the supplementary material.

Geometry and Operating Conditions

Flue gas side

The complete geometry of the convection section (see Figures 1 and 2) has been implemented in Fluent.[15] The former is indispensable as it is the intention to perform a coupled simulation of the complete flue gas side and the process gas side, while no symmetry walls can be introduced. While the radiation section can be considered as an empty box with one or two rows of coils in the middle, the convection section is more complicated from a geometrical point of view. The flue gas flow is driven over the tubes, resulting in heat transfer toward the process gas side, and leaves the convection section through the chimneys. Taking into account the possible changes in flow direction forced by the horizontally suspended tubes in the convection section, the description of the position and dimensions of all tubes should be accurate and up-to-date. The computational domain at the flue gas side of the convection section is divided into 1,959,806 hexahedral cells.

Due to the geometrical configuration of a steam cracking furnace (see Figure 1), the flue gas flow field at the convection section inlet is asymmetrical. Consequently, an additional simulation is carried out to determine the flue gas flow field in the bridgewall, that is the horizontal crossing from the radiation section to the convection section (see Figure 1). Next, the calculated velocity magnitude, x, y and z velocities, the turbulent kinetic energy and its dissipation rate at the bridgewall are implemented as initial boundary conditions in the simulation of the convection section. Based on industrial data, the flue gas temperature is given a value of 1450 K at the inlet of the convection section.[3] The polynomial functions, implemented in Fluent, to calculate the physical properties of the flue gas are available in Table S1 of the Supplementary Material.

Vaporizer

A Fluent simulation of the vaporizer is momentarily performed. This simulation is too time-consuming to present simulation results here. From an Aspen simulation it is calculated that 70% of the hydrocarbon feed is evaporated. From a heat balance, it is calculated that this fraction of evaporated feed rises to a value of 98% when mixed with the overheated steam. The hydrocarbon-steam mixture enters the mixture over-heater 1 as a spray flow.

The first results of these extremely time-consuming simulations of the vaporizer are presented by De Schepper et al.[36]

Steam over-heater

In the steam over-heater, the overheating of steam is simulated. One tube in this heat exchanger is made out of three horizontal passes, each with a length of 11.3 m and a diameter of 0.0779 m. The three horizontal passes are connected by two vertical bends. The complete 3-D-computational domain is divided into 856,953 hexahedral cells. Steam with a temperature of 447 K is fed at the tube inlets of the steam over-heater. The mass flow rate per tube is 0.3195 kg/s. The fluid pressure at the tube inlet is set to 403.5 kPa. The polynomial functions, implemented in Fluent, to calculate the physical properties of the steam are available in Table S2 of the Supplementary Material.

Mixture over-heater 1

One tube in the mixture over-heater 1 is made out of three horizontal passes, each with a length of 11.3 m and a diameter of 0.0779 m. These three passes are connected by two vertical bends. The complete 3-D-computational domain is divided into 1,764,315 hexahedral cells. A mixture of hydrocarbons and steam with a mass flow rate of 1.118 kg/s is fed at the tube inlets of the mixture over-heater 1. The fluid pressure at the different tube inlets is set to 349 kPa. At the inlet of one heat exchanger tube, uniform profiles for all the variables are imposed. These values are mass-averaged values obtained from the outlet values for the corresponding steam over-heater and vaporizer tubes. According to the tube under consideration, a different inlet temperature of the hydrocarbon-steam mixture, calculated with Aspen as described in the section Physical Properties, is, thus, imposed. The polynomial functions, implemented in Fluent, to calculate the physical properties of the hydrocarbon-steam mixture are available in Table S3 of the Supplementary Material.

Mixture over-heater 2

Two different tube geometries must be distinguished in mixture over-heater 2 (see Figure 2). Each tube of these two geometries consists of four horizontal passes, with a length

of 11.3 m and a diameter of 0.1023 m. These four passes are connected by two vertical bends and one oblique bend. If one follows the symbols in Figure 2, it can be seen that the two last passes of the heat exchanger tubes are geometrically noncorresponding. As a result, two possible geometries with either a large or small oblique bend can be observed. To establish the connection with the mixture over-heater 1, the vertical bend connecting both mixture over-heaters is also included in the geometry for the eight tubes. The complete 3-D-computational domain is divided into 2,962,120 and 2,974,811 hexahedral cells for the two possible geometries. The inlet conditions of a tube in this heat exchanger correspond to the outlet conditions of the corresponding tube in mixture over-heater 1. More specifically, at the inlet of these heat exchanger tubes, the outlet velocity and outlet temperature profile of the mixture over-heater 1 tubes are imposed. The polynomial functions, implemented in Fluent, to calculate the physical properties of the hydrocarbon-steam mixture are available in Table S4 of the Supplementary Material.

Boundary Conditions

The thermal boundary conditions are briefly presented. A temperature boundary condition is used for each flue gas side simulation, i.e., the inner tube wall temperature calculated in the simulations of the heat exchanger tubes.

In order to calculate the overheating of the steam and hydrocarbon-steam mixture in the heat exchanger tubes, the correct heat-flux profile must be imposed as thermal boundary condition at the tube wall boundaries. These heat fluxes have been determined based on CFD calculations of the flue gas flow and temperature field over the heat exchanger tubes in the convection section box, as described in the previous paragraph. By this approach, a vertical coupling between the flue gas side and process gas side is achieved. The bends, connecting the horizontal straight passes, are located outside the convection section box. A zero heat flux is defined as boundary condition for these bends, thus assuming a perfect insulation. By imposing a varying heat-flux profile on the wall of each heat exchanger tube (over the eight different positions, see Figure 2), the influence of the position of the heat exchanger tube in the convection section box on the calculated temperature field is investigated.

Numerical Procedures

The calculations are performed making use of a second-order upwind calculation scheme[20] for the determination of momentum, energy, turbulent kinetic energy k and dissipation of turbulent kinetic energy ε. For the flue gas side, the SIMPLE algorithm[37] is applied for the pressure-velocity coupling. For the simulations of the process gas side, the PISO algorithm[38] is used for the coupling of pressure and velocity.

The convergence is based on the residual value of the calculated variables, namely mass, velocity components, temperature, k and ε. In the presented calculations, the numerical computation is considered to be converged when the scaled residuals of the variables mass, velocity components, k and ε have lowered by four-orders of magnitude, and when the residuals of the temperature variable have lowered by six-orders of magnitude.

Simulation Results

Flue gas side

The main interest of the simulation of the flue gas side is the calculation of the correct flow and temperature field of the flue gas flowing over the convection section tubes, and, hence, of the correct heat-flux profiles on the tube walls. Furthermore, a complete description of the flue gas conditions at the outlet of the steam cracking furnace is obtained.

The flue gas velocity magnitude field is depicted in Figure 4. An asymmetrical distribution of the flue gas can be observed under the lowest tube row. Moreover, under the lowest tube row at the side of the bridgewall, a large stagnant zone can be seen. After passing the two lower tube rows, the flue gas flow becomes more uniform and better dispersed between the tubes. A reorganization of the flow is seen between the steam over-heater and the vaporizer due to a change in the internal geometry that is a change in width of the convection section box. As the flue gas passes the vaporizer, the flue gas flow already turns inwards to the chimneys.

The temperature field of the flue gas in the convection section is also depicted in Figure 4. The temperature of the flue gas below the first tube row is the highest in the zone where the velocity magnitude is the highest. Further downstream, the temperature decreases uniformly as it is distributed between the tubes as discussed in the previous paragraph. However, small differences in the temperature field are observed between the left and righthand side of the convection section. The highest values are calculated at the side opposite the bridgewall opening. This is caused by the specific flow field under the lower heat exchanger tubes, where more flue gas flows to the left side of the convection section, as discussed before. A flue gas outlet temperature of 883 K is calculated. In the industrial steam cracking furnace, an outlet temperature of 896 K was measured. Consequently, the calculated value is in good agreement with the measured value.

Figure 5 represents the calculated heat-flux profiles on the walls of the heat exchanger tubes. It must be remarked that the displayed values for the heat fluxes are negative since the heat is transferred from the flue gas side to the process gas side. It can be seen that the distribution of heat transferred from the flue gas to the tube skin is quite uniform over the different heat exchanger tubes, except for the lower three tube rows, where more extreme values are calculated. These high wall heat fluxes are due to radiation from the flue gas and the side walls to the tube skins. As seen in Figure 4, the flue gas temperatures under the lower tubes are high enough for a considerable radiation effect. A maximum heat flux of 169 kW/m^2 is calculated for the lowest tube row. For this tube row, 80% of the heat transfer is radiative. The lowest values of heat fluxes are of the order of 10 kW/m^2, and are calculated for the heat exchanger tubes of the steam over-heater. This is explained by the smaller temperature difference between flue gas and tube skin, resulting in a lower driving force for convective heat transfer.

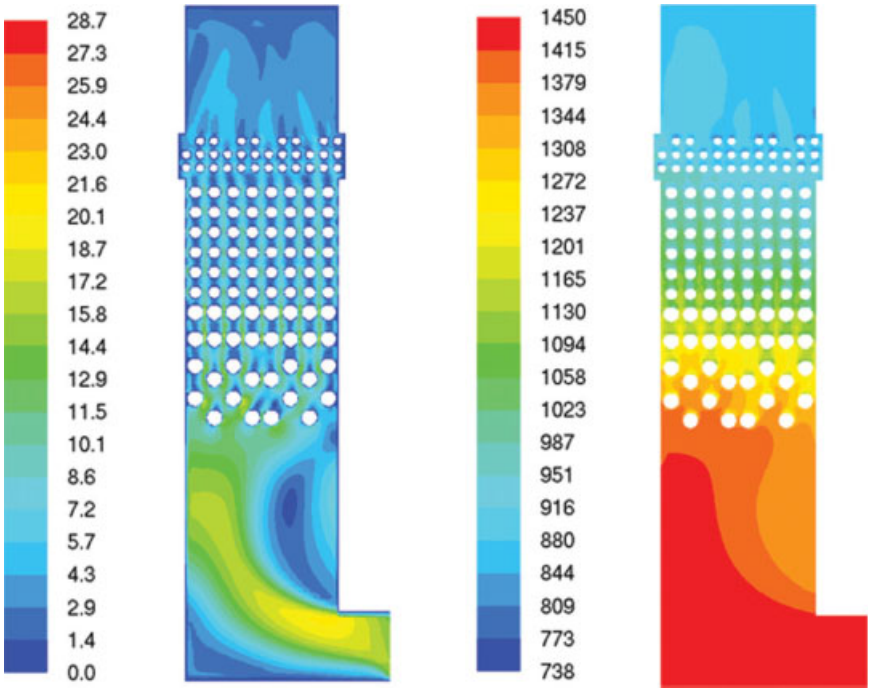

Figure 4. Velocity magnitude field [m/s], and temperature field [K] of the flue gas in the convection section.

A comparison of the heat fluxes calculated around the tube walls of the first row of the mixture over-heater 1 is shown in Figure 6. In this figure, different positions on one hand and different zones on each tube on the other hand are presented. First, it can be seen that the calculated heat-flux profile differs from tube to tube. The lowest heat fluxes are calculated for the tubes located in the middle of the convection section, positions 4-5-6 in Figure 2. The highest heat fluxes are observed on the tube located in position 1. Moreover, a very high heat flux is calculated on the left hand side of this tube, that is the tube side facing the convection section wall. This can be explained by radiative heat transfer from this wall. The same is observed on the tube located in position 8, where the highest heat flux is now calculated on the righthand side of the tube.

When comparing the different zones on a single tube, it can be seen that the heat fluxes on the left and righthand side are always higher than the heat fluxes on the top and down side. This can be explained by the flue gas velocity field presented in Figure 4. The flue gas velocity at the left and righthand side of the tube is always higher than above and below the tube, implying that the convective heat transfer in the former positions is higher than in the latter

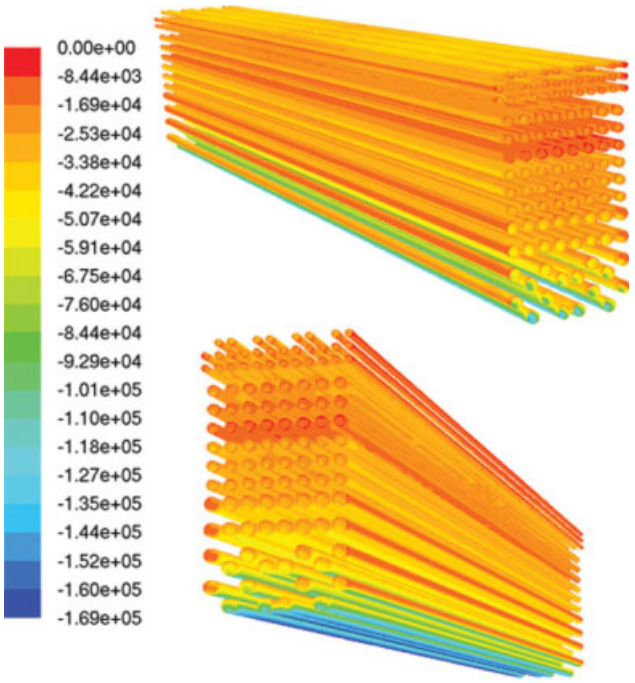

Figure 5. Heat flux profiles [W/m^2] on the heat exchanger tubes.

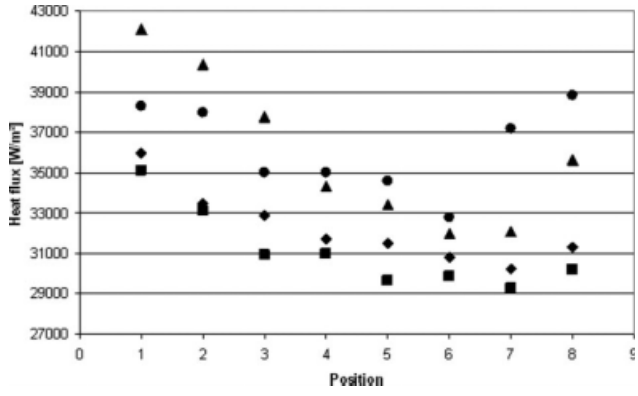

Figure 6. Calculated heat fluxes [W/m^2] on the tube walls of the first row of the mixture over-heater 1 (◆ top, ■ down, ▲ left, ● right).

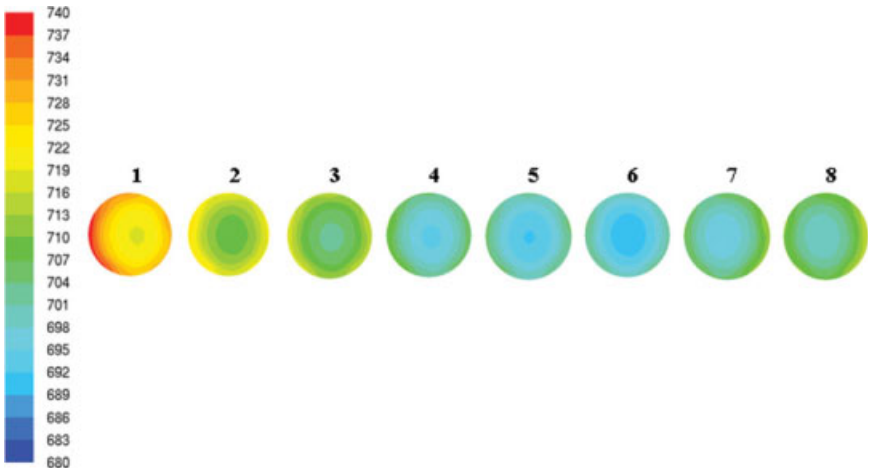

Figure 7. Temperature field [K] of the steam at the outlet of the eight heat exchanger tubes of the steam over-heater.

positions. The differences between the heat fluxes on the top and down side are quite small.

Considering the total heat input in a steam cracking furnace, it is calculated that 43% of this heat is transferred from the flue gas to the reactor coils in the radiation section,[3] while 52% is transferred from the flue gas to the heat exchanger tubes in the convection section. Consequently, 5% of the total heat input in the radiation section is lost via the chimney.

Steam over-heater

Figure 7 gives an overview of the calculated temperature fields at the outlet of the eight heat exchanger tubes in the steam over-heater. The outlet planes shown in Figure 7 correspond with the outlets of the tubes located in row 3 of the steam over-heater, see Figure 2. As can be seen on Figure 2, position 1 corresponds with the tube closest to the furnace wall opposite to the bridgewall opening.

The position of the heat exchanger tube indeed influences the steam outlet temperature. The lowest heat-flux profiles are calculated for the central tubes, see Figure 5, resulting in the lowest outlet temperatures for the steam. Furthermore, the heat-flux profiles on the tubes located at the convection section side facing the bridgewall, i.e., positions 1 and 2 in Figure 2, are much higher than the ones located on positions 7 and 8. The only explanation for this is that the influence of the asymmetric inlet flow field of the flue gas is still felt in the steam over-heater. Thus, the position of the heat exchanger tube does influence the outlet temperature of the steam, and it is not allowed to assume that the operating conditions for all steam over-heater tubes are the same. According to the tube under consideration, the steam will have a higher or lower outlet temperature. Off course, this will also have an influence on the temperature of the hydrocarbon-steam mixture at the inlet of the mixture over-heater 1. Consequently, for an accurate simulation of the phenomena in the convection section, all heat exchanger tubes should be calculated based on a specific heat-flux profile for that tube, to be used as boundary condition. The latter profile is determined from a simulation of the flue gas side of the convection section.

The temperature increase of the steam along the eight tubes of the steam over-heater is shown in Figure 8. The mass-averaged temperatures, shown in this Figure, are computed by dividing the summation of the products of the temperature and mass flux in each computational cell by the total mass flux. Steam with a temperature of 447 K is fed to the eight tubes. As the steam flows further down through the tube, its temperature increases. However, due to the different heat-flux profiles imposed on the tube walls, different temperature profiles are calculated depending on the position of the tube in the convection section. The highest outlet temperature is observed for position 1, while the steam has the lowest outlet temperature in position 6. The difference between the highest and lowest temperature is 30 K. A mean outlet temperature of 706 K when averaging out over the eight heat exchanger tubes is calculated.

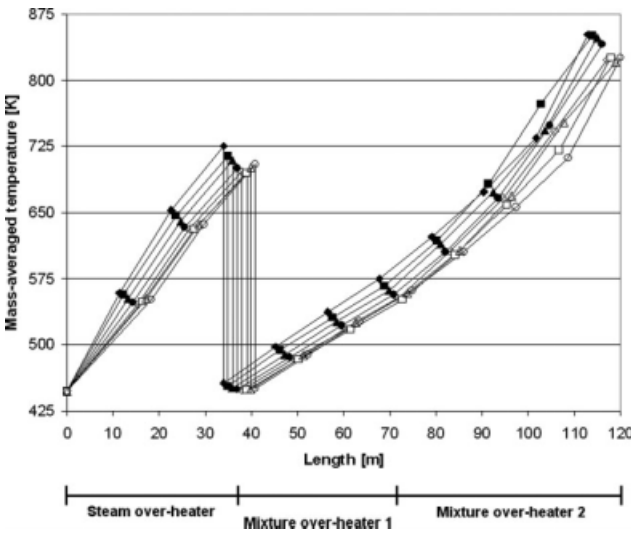

Figure 8. Mass-averaged temperature [K] of the steam and hydrocarbon-steam mixture in the eight different tubes of the heat exchangers (1: ◆, 2: ■, 3: ▲, 4: ●, 5: ◇, 6: □, 7: Δ, 8: ○).

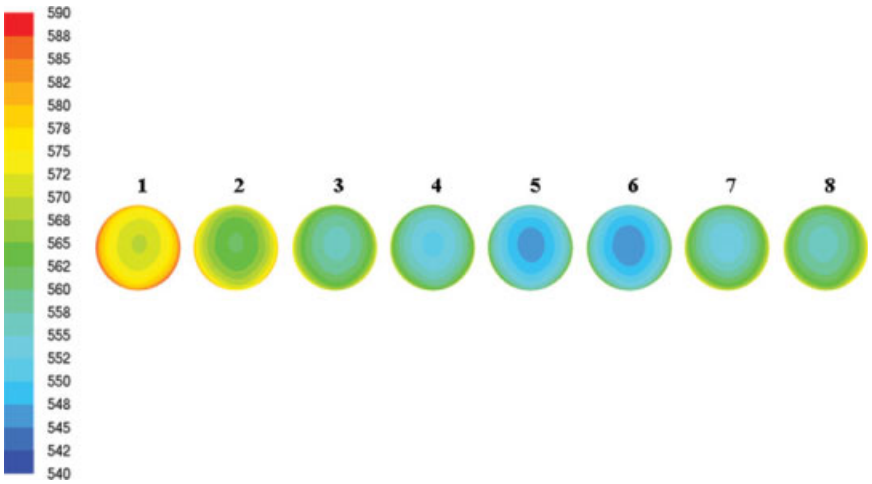

Figure 9. Temperature field [K] of the hydrocarbon-steam mixture at the outlet of the eitht heat exchanger tubes of the mixture over-heater 1.

The main interest of the simulation of the steam over-heater is the calculation of the correct flow and temperature field of the steam flowing through the eight tubes. Following these results, the tube skin temperature fields are determined. It has been found that the tube skin temperature ranges from 450 K to 800 K. At the inlet of the tube, the lowest tube skin temperature is observed. As the steam temperature in the different tubes increases, the tube skin temperature increases as well. During the flue gas side simulations, these temperature fields are used as thermal boundary condition.

As mentioned before, the outlet temperature of the steam will influence the inlet temperature of the hydrocarbon-steam mixture in the next heat exchanger. With the above obtained outlet temperatures for the steam, the inlet temperatures for the hydrocarbon-steam mixture in the mixture over-heater 1 have been determined. These temperatures are considered as inlet conditions for the simulation of the mixture over-heater 1 tubes, discussed in the next section.

Mixture over-heater 1

In this heat exchanger, the hydrocarbon-steam mixture is further vaporized and overheated. Again, the influence of the position of the heat exchanger tube on the temperature field of the hydrocarbon-steam mixture is investigated.

Figure 9 gives an overview of the temperature fields at the outlet of the eight heat exchanger tubes. The outlet planes, shown in Figure 9, correspond with the outlets of the tubes located in row 1.3 of mixture over-heater 1, see Figure 2. Position 1 corresponds with the tube closest to the convection section wall opposite to the bridgewall opening. The position of the heat exchanger tube indeed has a significant influence on the calculated outlet temperature. For example, a mass-averaged outlet temperature of 575 K is calculated for the tube located in position 1, while this value is 552 K for the tube located in position 6. The heat-flux profiles for the tubes in the middle of the heat exchanger are the lowest, as can be seen on Figure 5, resulting in the lowest outlet temperatures for the hydrocarbon-steam mixture. Again, the asymmetric inlet flow field of the flue gas in the convection section in combination with the radiation from the flue gas and the convection section wall significantly influences the calculation results.

The temperature increase of the hydrocarbon-steam mixture along the eight tubes of the mixture over-heater 1 is shown in Figure 8. Since different outlet temperatures are calculated for each tube of the steam over-heater, see Figure 8, eight different inlet temperatures for the mixture over-heater 1 tubes are imposed. As the hydrocarbon-steam mixture flows through the tube, its temperature increases. However, due to the different heat flux profiles imposed on the tube walls, different temperature profiles are calculated depending on the position of the tube in the convection section. The highest outlet temperature is observed for position 1, while the lowest outlet temperature corresponds with position 6. The temperature differences between the eight different tubes further grow, but the relative position of the curves remains the same. A difference of 24 K in outlet temperatures for the different positions is calculated. From these results, a mean outlet temperature of 560 K can be derived.

As for the steam over-heater, the internal tube skin temperature profiles for the mixture over-heater 1 have also been determined. For this heat exchanger, the tube skin temperatures vary between 450 K and 700 K. Again, for all tubes it is found that the tube skin temperature increases as the mixture temperature increases. The calculated temperature profiles are important since they are used as thermal boundary conditions in the flue gas side simulation.

The simulation results for mixture over-heater 1 are currently being used to perform an Eulerian-Lagrangian simulation in which the trajectories of the spray flow droplets in the tubes are calculated. Their impact behavior on the tube walls is combined with a coking model to simulate the fouling in the tubes. The results of these simulations will be presented soon. The first simulation results seem to correspond well with the available industrial data. Once the final simulation results for tube fouling are obtained, they will be used to optimize the convection section geometry.

Mixture over-heater 2

In this heat exchanger, the hydrocarbon-steam mixture is further overheated. The influence of the position of the heat

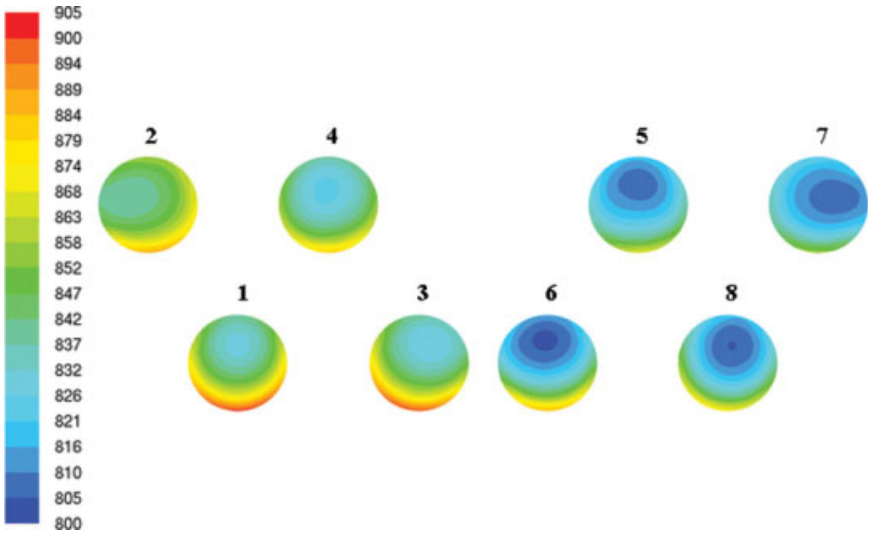

Figure 10. Temperature field [K] of the hydrocarbon-steam mixture at the outlet of the 8 heat exchanger tubes of the mixture over-heater 2.

exchanger tube on the temperature field of the hydrocarbon-steam mixture is again investigated.

Figure 10 gives an overview of the temperature fields at the outlet of the eight heat exchanger tubes. As can be seen in Figure 2, the outlets of positions 1, 3, 6 and 8 are located in the lowest tube row, situated in the convection section. Consequently, a very high heat flux is calculated for the lower tube walls. At these positions, very high-temperatures are observed. However, due to the asymmetric inlet profile of the flue gas in the convection section, a difference can again be seen between the tubes located on the side facing the bridgewall (Figure 2: positions 1 and 3), and the tubes located near the bridgewall (positions 6 and 8). Furthermore, the flue gas flows directly over the tubes located on position 1 and 3, causing a higher heat flux due to convection, and, thus, temperature inside these tubes.

For the tubes located in the second lowest tube row (positions 2, 4, 5 and 7) having a lower heat flux on their tube walls as can be seen in Figure 5, lower outlet temperatures are calculated. The tubes located in the second lowest tube row of the convection are as it were "protected" from the direct radiation of the flue gas by the tubes located in the lowest tube row. Again, also in this tube row, a difference in outlet temperature is observed according to the position in the convection section: positions 2 and 4 have a higher outlet temperature since they are located in the direct flow of the flue gas.

The temperature increase of the hydrocarbon-steam mixture along the eight tubes of the mixture over-heater 2 is shown in Figure 8. As mentioned before, the inlet conditions for the simulations of the mixture over-heater 2 are the calculated outlet conditions of the mixture over-heater 1, see Figures 8 and 9. As the hydrocarbon-steam mixture flows through the tubes, its temperature increases. However, due to the different heat-flux profiles imposed on the tube walls, different temperature profiles are calculated depending on the position of the tube in the convection section. Contrary to the results of the steam over-heater and mixture over-heater 1, the profiles for this heat exchanger are less smooth. The influence of the asymmetric flow field of the flue gas coming from the radiation section (see Figure 4), in combination with the radiation from the flue gas and the convection section wall can be clearly seen. The heat-flux profiles on the tubes located in the convection section facing the bridgewall (position 1-2-3-4) are much higher than the ones located at the opposite side (position 5-6-7-8): typically 169 kW/m^2 vs.120 kW/m^2. This results in higher outlet temperatures for the hydrocarbon-steam mixture. From these results, a mean outlet temperature of 836 K is calculated. In the industrial steam cracking furnace, an outlet temperature of 876 K was measured. Consequently, the calculated value is in reasonable agreement with the measured value.

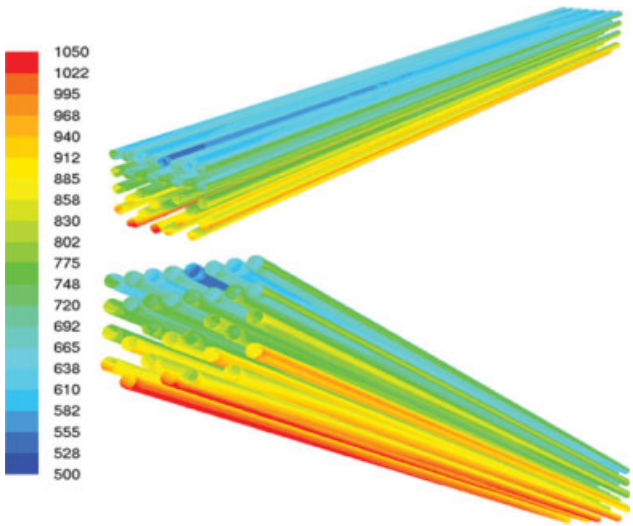

Figure 11. Internal tube skin temperature fields [K] of mixture over-heater 2.

In Figure 11, the calculated internal tube skin temperature fields are visualized for the eight different tubes of the mixture over-heater 2. The tube inlet positions for this heat exchanger are alternating over the two opposite sides of the convection section walls. This is also true for the other heat exchangers. However, the tube skin temperature fields have not been visualized for the steam over-heater and the mixture over-heater 1. Due to the alternating position of the inlets, the calculated temperature fields are also alternating in the convection section. Remark that very high internal tube skin temperatures of about 1050 K are calculated for the lowest pass of the tube located in position 1 and 3. Again, this is explained by the asymmetric inlet flow field of the hot flue gas coming from the radiation section. This asymmetry is the strongest at this position as also observed in the calculated temperature fields. The coupled simulation of the convection section has thus revealed the presence of hot spots on the tubes located in the lowest tube row of the convection section. Possibly, these hot spots may be related to the fouling problems appearing in the convection section.

As for mixture over-heater 1, a further simulation of mixture over-heater 2 will be performed combining the heat-transfer effect with an appropriate coking model. The obtained results will be presented soon and used for a further optimization of the convection section geometry.

Conclusions

A coupled simulation of the entire convection section of an industrial steam cracker is performed to identify the convection section zones vulnerable for possible cokes formation. By performing the coupled simulation, all velocity and temperature fields in the different heat exchangers and for the flue gas are determined, accounting for the best applicable turbulence model.

The influence of the asymmetric inlet flow field of the flue gas in the convection section is felt over the complete height of the convection section that is by all heat exchangers. As a result, the outlet temperatures of the tubes located in the convection section facing the bridgewall are higher than the ones of the tubes located at the opposite side. Additionally, for the tubes located near the convection section wall, higher heat-flux profiles are calculated on the tube wall zones facing the convection section wall due to radiative heat transfer. The calculated heat flux profiles for the different tubes in one tube row clearly differ. Consequently, it cannot be assumed that the variation of the flow and temperature fields in the different tubes of one type of heat exchanger is the same. Large differences in outlet temperatures of the hydrocarbon-steam mixture leaving the convection section, are, thus, observed. The calculated outlet temperatures range from 820 K to 852 K. Hence, a complete simulation considering each tube in the convection section is required to obtain reliable results.

Very high-internal tube skin temperatures up to 1050 K are calculated for the tubes in the lowest tube row and facing the bridgewall. The coupled simulation of the convection section, thus, reveals the presence of hot spots on a number of tubes, possibly causing fouling problems in these tubes.

The industrially observed fouling problems in mixture over-heater 1 and mixture over-heater 2 are momentarily being investigated based on the calculated velocity and temperature profiles, using all appropriate simulation models. The results will be used to optimize the convection section geometry and operating conditions. They will be reported soon.

Notation

Roman letters

C_{ij} = convection contribution, kg/m^{3}s
$C_{1\varepsilon}$ = standard and RNG k-ε model constant
$C_{2\varepsilon}$ = standard and RNG k-ε model constant
C_μ = standard and RNG k-ε model constant
C_v = RNG k-ε model constant $C_v \approx 100$
$D_{L,ij}$ = molecular diffusion contribution with $(i, j) \in (x, y, z)$, kg/m^{3}s
$D_{T,ij}$ = turbulent diffusion contribution with $(i, j) \in (x, y, z)$, kg/m^{3}s
E = total energy per unit mass, J/kg
G_{ij} = buoyancy production contribution with $(i, j) \in (x, y, z)$, kg/m^{3}s
k = turbulent kinetic energy, J/kg
P_{ij} = stress production contribution with $(i, j) \in (x, y, z)$, kg/m^{3}s
p = pressure Pa
q_j = conductive heat flux in the x_j – direction, J/m^{2}s
S_E = source term in the energy equation, J/m^{3}s
S_F = source term in the momentum conservation equation, kg/m^{2}s^2
S_M = source term in the mass conservation equation, kg/m^{3}s
t = time, s
u_i = velocity component in the x_i – direction, m/s
$\overline{u}_i$ = Reynolds average of u_i, m/s
$\overline{u}_i$ = Reynolds fluctuation of u_i, m/s
uj = velocity component in the x_j – direction, m/s
$\overline{u}_j$ = Reynolds average of u_j, m/s
u_j' = Reynolds fluctuation of u_j, m/s
x_i = x$_i$-direction or coordinate, with $i \in (x, y, z)$, m
x_j = x_j-direction or coordinate, with $j \in (x, y, z)$, m

Greek letters

δ_{ij} = Kronecker function
ε = viscous dissipation of turbulent kinetic energy, m^2/s^3
ε_{ij} = dissipation term with $(i, j) \in (x, y, z)$, kg/m^{3}s
μ = dynamic viscosity, Pa s
μ_k = dynamic viscosity of phase k, Pa s
μ_{turb} = turbulent viscosity, Pa s
ρ = density, kg/m^3
ρ_k = density of phase k, kg/m^3
σ = turbulent Prandtl number
σ_k = standard and RNG k-ε model constant
σ_ε = standard and RNG k-ε model constant
τ = viscous stresses with $(i, j) \in (x, y, z)$, kg/ms^2
φ_{ij} = pressure strain term with $(i, j) \in (x, y, z)$, kg/m^{3}s

Literature Cited

1. Gal T, Lakatos BG. Thermal cracking of recycled hydrocarbon gas-mixtures for re-pyrolysis: Operational analysis of some industrial furnaces. *Appl Therm Eng*. 2008;28:218–225.
2. Van Geem KM, Heynderickx GJ, Marin GB. A comparison of one and two-dimensional reactor models for steam cracking: effect on yields and coking rate. *AIChE J*. 2004;50:173–183.
3. Heynderickx GJ, Oprins AJM, Dick E, Marin GB. Three-dimensional flow patterns in cracking furnaces with long-flame burners. *AIChE J*. 2001;47:388–400.
4. Stefanidis GD, Heynderickx GJ, Marin GB. CFD simulations of steam cracking furnaces using detailed combustion mechanisms. *Comput Chem Eng*. 2006;30:635–649.
5. Lan X, Gao J, Xu C. Numerical simulation of transfer and reaction processes in ethylene furnaces. *Chem Eng Res Des*. 2007;85:1565–1579.
6. Han YL, Xiao R, Zhang MY. Combustion and pyrolysis reactions in a naphtha cracking furnace. *Chem Eng Technol*. 2007;30:112–120.

7. Rao MVR, Plehiers PM, Froment GF. The coupled simulation of heat transfer and reaction in a pyrolysis furnace. *Chem Eng Sci*. 1988;43:1223–1229.
8. Masoumi ME, Sadrameli SM, Towfighi J. Simulation, optimization and control of a thermal cracking furnace. *Energy*. 2006;31:516–527.
9. Ghashghaee M, Karimzadeh R. Dynamic modeling and simulation of steam cracking furnaces. *Chem Eng Technol*. 2007;30:835–843.
10. Cai H, Krzywicki A, Oballa MC. Coke formation in steam crackers for ethylene production. *Chem Eng Process*. 2002;41:199–214.
11. Wauters S, Marin GB. Kinetic modeling of coke formation during steam cracking. *Ind Eng Chem Res*. 2002;41:2379–2391.
12. Souza BA, Matos EM, Guirardello R, Nunhez JR. Predicting coke formation due to thermal cracking inside tubes of petrochemical fired heaters using a fast CFD formulation. *J Pet Sci Eng*. 2006; 51:138–148.
13. Heynderickx GJ, Froment GF. Simulation of the run length of an ethane cracking furnace with reactor tubes of circular and elliptical cross section. *Ind Eng Chem Res*. 1998;37:914–922.
14. Aspen Plus, Version 12.1. Ten Canal Park, Cambridge (MA) 02141: Aspen Technology, Inc.; 2004.
15. Fluent, Inc. *Fluent 6.3 User's Guide*. 2006; Lebanon, USA.
16. Dhir VK. Boiling heat transfer. *Ann Rev Fluid Mech*. 1998;30:365–401.
17. Ghorai S, Nigam KDP. CFD modeling of flow profiles and interfacial phenomena in two-phase flow in pipes. *Chem Eng Process*. 2006;45:55–65.
18. De Schepper SCK, Heynderickx GJ, Marin GB. CFD modeling of all gas-liquid and vapor-liquid flow regimes predicted by the Baker chart. *Chem Eng J*. 2008;138:349–357.
19. Anderson JD. *Computational Fluid Dynamics: The Basics with Applications*. New York, McGraw-Hill; 2005.
20. Versteeg HK, Malalasekera W. *An Introduction to Computational Fluid Dynamics, The Finite Volume Method*. Harlow, Essex, U.K: Longman Scientific and Technical; 1995.
21. Launder BE, Spalding DB. *Lectures in Mathematical Models of Turbulence*. London, U.K: Academic Press; 1972.
22. Yakhot V, Orszag SA. Renormalization group analysis of turbulence i. basic theory. *J Sci Comput*. 1986;1:3–51.
23. Yakot V, Orszag SA, Thangam S, Gatski TB, Speziale CG. Development of turbulence models for shear flows by a double expansion technique. *Phys Fluids A*. 1992;4:1510–1520.
24. Ranade VV. *Computational Flow Modeling for Chemical Reactor Engineering*, Volume 5. St Louis, MO: Academic Press; 2002:5.
25. Adzhemyan LT, Antonov NV, Vasiliev AN. *The Field Theoretic Renormalization Group in Fully Developed Turbulence*. London, U.K.: Gordon and Breach Science Publishers; 1999.
26. Pruvost J, Legrand J, Legentilhomme P. Numerical investigation of bend and torus flows, part I: effect of swirl motion on flow structure in U-bend. *Chem Eng Sci*. 2004;59:3345–3357.
27. Habibi A, Merci B, Heynderickx GJ. Impact of radiation models in CFD simulations of steam cracking furnaces. *Comput Chem Eng*. 2007;31:1389–1406.
28. Gibson MM, Launder BE. Ground Effects on Pressure Fluctuations in the Atmospheric Boundary Layer. *J Fluid Mech*. 1978;86:491–511.
29. Cortes C, Gil A. Modeling the gas and particle flow inside cyclone separators. *Prog Energy Combust Sci*. 2007;33:409–452.
30. Hidayat M, Rasmuson A. Numerical assessment of gas-solid flow in a U-bend. *Chem Eng Res Des*. 2004;82:332–343.
31. Udaya Bhaskar K, Rama Murthy Y, Ravi Raju M, Sumit Tiwari, Srivastava JK, Ramakrishnan N. CFD simulation and experimental validation studies on hydrocyclone. *Miner Eng*. 2007;20:60–71.
32. Kim TY, Baek SW. Analysis of combined conductive and radiative heat transfer in a two-dimensional rectangular enclosure using the discrete ordinates method. *Int J Heat Mass Transfer*. 1991;34: 2265–2273.
33. Truelove JS. Discrete-ordinate solutions of the radiative transport equation. *ASME J Heat Transfer*. 1987;109:1048–1051.
34. Hottel HC, Mangelsdorf HG. Heat transmission by radiation from non-luminous gases II. Experimental study of carbon dioxide and water vapour. *Trans Am Inst Chem Eng*. 1935;31:517–549.
35. Leckner B. Spectral and total emissivity of water vapor and carbon dioxide. *Combust Flame*. 1972;19:33–48.
36. De Schepper SCK, Heynderickx GJ, Marin GB. Modeling the evaporation of a hydrocarbon feedstock in the convection section of a steam cracker. *Comput Chem Eng*. 2009;33:122–132.
37. Patankar SV, Spalding DB. A calculation procedure for heat, mass and momentum transfer in three-dimensional parabolic flows. *Int J Heat Mass Transfer*. 1972;15:1787–1806.
38. Issa RI. Solution of the implicitly discretized fluid flow equations by operator splitting. *J Comput Phys*. 1986;62:40–65.

Manuscript received July 14, 2008, and revision received Mar. 23, 2009.